SCIENCE CHINA
Information Sciences

• RESEARCH PAPER •

August 2024, Vol. 67, Iss. 8, 182402:1–182402:10
https://doi.org/10.1007/s11432-023-3932-2

Tuning the ferroelectricity of $Hf_{0.5}Zr_{0.5}O_2$ with alloy electrodes

Keqin LIU[1], Bingjie DANG[1], Zhiyu YANG[2], Teng ZHANG[1], Zhen YANG[1], Jinxuan BAI[1], Zelun PAN[1], Ru HUANG[1,3] & Yuchao YANG[1,2,3,4*]

[1]*Beijing Advanced Innovation Center for Integrated Circuits, School of Integrated Circuits, Peking University, Beijing* 100871*, China;*
[2]*School of Electronic and Computer Engineering, Peking University, Shenzhen* 518055*, China;*
[3]*Center for Brain Inspired Chips, Institute for Artificial Intelligence, Peking University, Beijing* 100871*, China;*
[4]*Center for Brain Inspired Intelligence, Chinese Institute for Brain Research, Beijing, Beijing* 102206*, China*

Received 15 August 2023/Revised 6 October 2023/Accepted 4 January 2024/Published online 15 July 2024

Abstract Tuning ferroelectricity of $Hf_{0.5}Zr_{0.5}O_2$ is crucial for facilitating its practical applications in various fields, including in-memory and neuromorphic computing. Previous studies have revealed that the electrodes have a significant influence on ferroelectricity, and changing electrode materials can realize different but discrete ferroelectric polarization values. Here, we introduce an alloy-electrode method, in order to achieve gradual and accurate modulation of ferroelectric polarization, especially useful for matching the polarization charges at the interface of ferroelectric insulators and ferroelectric semiconductors. Au and W electrodes are chosen as baselines for realizing weak and strong ferroelectric polarization, where the intermediate states can be achieved by adjusting the ratio of metals in the Au-W alloy. To demonstrate the generality of this approach, the Cu-W alloy electrode is also realized for tuning ferroelectric polarization. The effect of alloy electrodes on device leakage current, endurance, and retention is evaluated. In addition, the temperature stability of ferroelectric capacitors is tested, where limited changes in both remnant polarization and coercive voltages are observed, showing the great potential of the ferroelectric hafnium oxide. Such gradual modulation of ferroelectric polarization could facilitate the application of $Hf_{0.5}Zr_{0.5}O_2$ in in-memory and neuromorphic computing.

Keywords ferroelectric hafnium oxide, alloy electrode, gradual modulation, temperature stability

1 Introduction

HfO_2-based ferroelectric materials have attracted great attention in recent years, due to their high CMOS compatibility and scalability [1, 2], holding great prospects in in-memory [3, 4], and neuromorphic computing [5–10]. Ferroelectricity and anti-ferroelectricity have been discovered in HfO_2 doped with different elements for different doping concentrations, such as Si [11, 12], Al [13, 14], Y [15, 16], and Zr [17–20], showing great potential in ferroelectric random-access memories (FRAMs) [21–23], ferroelectric field-effect transistors (FeFETs) [6,24], and ferroelectric tunnel junctions (FTJs) [25,26]. The ferroelectricity in HfO_2 stems from the non-centrosymmetric orthorhombic phase with a $Pca2_1$ space group [11,27,28]. The electrode materials [27, 29–33] and the rapid thermal annealing (RTA) process [19, 27] play very important roles in stabilizing the orthorhombic phase in HfO_2 films due to the mechanical confinement [34] under appropriate annealing conditions, which should be carefully considered. Different capping electrodes with varied thermal expansion coefficients (α) have been tested, which provide various strain conditions during the RTA process, resulting in different ferroelectric polarization [31]. However, the discrete α values for different materials lead to discrete ferroelectric polarization values, where the fine-tuning ability is hard to achieve.

With the development of ferroelectric semiconductors, the integration of ferroelectric semiconductors with ferroelectric insulators and further construction of Fe^2FETs becomes possible, where the matching of polarization charges is crucial [35]. Since emergent ferroelectric semiconductors are usually single

* Corresponding author (email: yuchaoyang@pku.edu.cn)

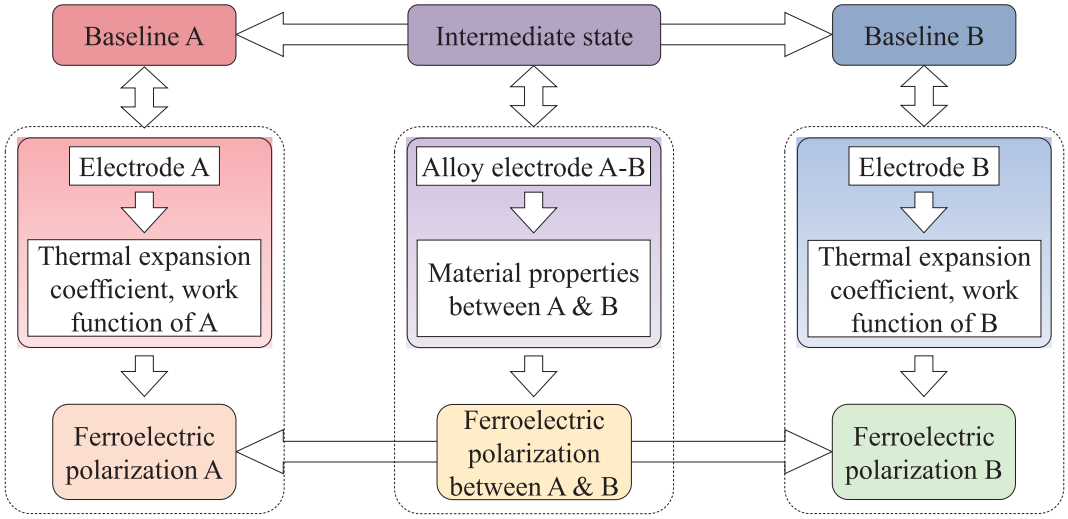

Figure 1 (Color online) Overall strategy of tuning ferroelectricity with alloy electrodes.

crystals with relatively fixed ferroelectric polarization [36, 37], the gradual and accurate modulation of ferroelectric polarization of HfO_2 becomes very important.

In this work, we introduce a novel alloy-electrode approach for gradually tuning the ferroelectricity between two baselines determined by two different capping materials. The baselines are set by using gold (Au) and tungsten (W) as capping electrodes, showing weak and strong ferroelectricity, respectively. Then, the Au-W alloy electrodes with different ratios are realized by changing the co-sputtering power. As the ratio of W increases, the remnant polarization (P_r) increases accordingly, demonstrating the fine-tuning ability. Cu-W alloy electrodes have also been realized, proving that the alloy-electrode method is a general way to tune the ferroelectric polarization. The influence of alloy electrodes on device leakage current, endurance, and retention is tested. Moreover, the temperature stability of the ferroelectric capacitors is investigated when temperature increases from 300 to 500 K. The $2P_r$ of $Hf_{0.5}Zr_{0.5}O_2$ (HZO) film only slightly decreases, owing to its high Curie temperature (T_c). The shift of coercive voltages is limited, due to the relatively inert electrodes. The fabricated capacitors also show a less significant imprint effect compared with capacitors using TiN electrodes.

2 Alloy-electrode method

The basic idea of tuning the ferroelectricity of HZO using alloy electrodes is illustrated in Figure 1. Firstly, two baselines are determined by two different materials as the top electrodes (TEs), where electrode A is less favorable for the formation of ferroelectricity while electrode B is more favorable. Since the $2P_r$ decreases as α increases [31], materials with large thermal expansion coefficients are good candidates for electrode A, and the opposite is suitable for electrode B. The bottom electrode and annealing condition are kept unchanged. Secondly, after determining the baselines, the ferroelectricity between baselines A and B can be achieved by gradually tuning the ratio of metals in the A-B alloy, which stems from the adjusted thermal expansion coefficient and strain condition of the top electrode.

3 Fabrication of alloy electrodes and their influence on ferroelectricity

In order to demonstrate this idea, the two-terminal ferroelectric capacitors in this work were fabricated on the heavily doped n-type Si substrate (0.002–0.004 $\Omega\cdot$cm). The bottom electrode (Au 60 nm/Ti 4 nm) was deposited on the Si substrate by electron beam evaporation. Afterward, HZO film was grown by atomic layer deposition (ALD) with a thickness of 17 nm. The top electrode was patterned by ultraviolet (UV) lithography, the size of which is 50 μm × 50 μm. Subsequently, 80 nm-thick Au, W, Cu, Au-W alloys or Cu-W alloys were deposited as top electrodes via magnetron sputtering, followed by the lift-off process. Finally, the fabricated devices were annealed for 60 s at 500 °C in a nitrogen atmosphere to enhance the ferroelectricity of the film. The device structure and fabrication process flow are shown in

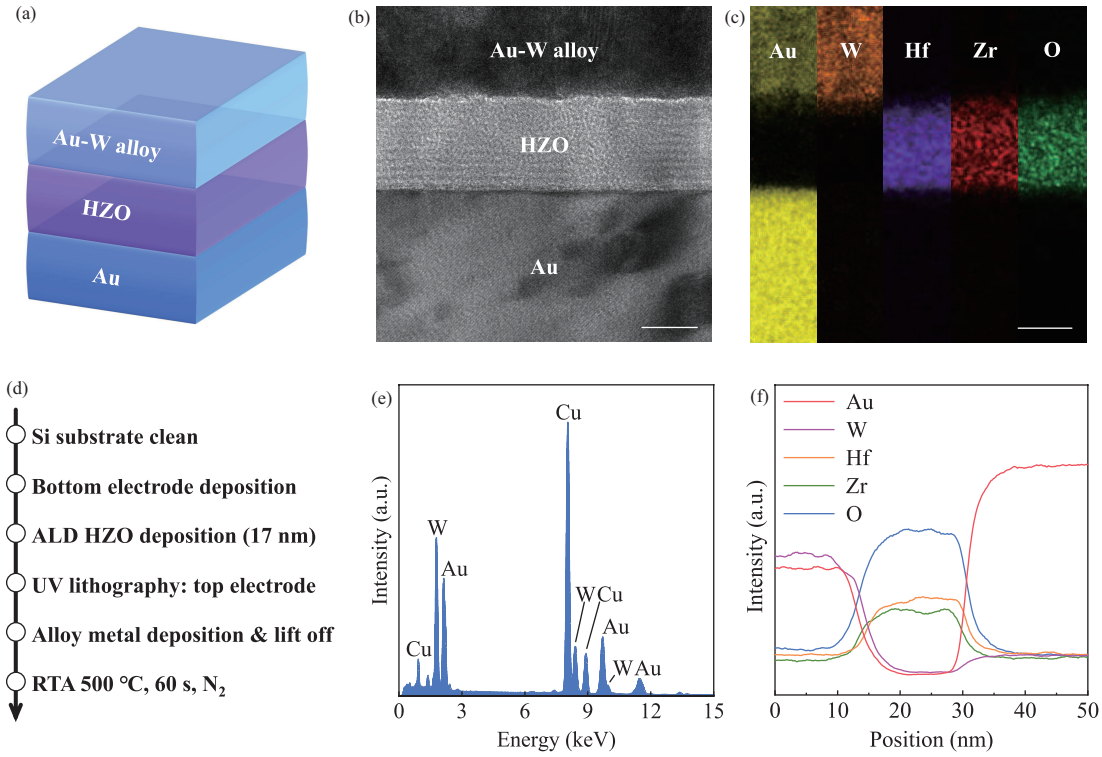

Figure 2 (Color online) (a) Schematic of the Au-W alloy/HZO/Au device structure. (b) Cross-sectional TEM image of the Au-W alloy/HZO/Au device. Scale bar: 10 nm. (c) EDS mapping of the Au-W alloy/HZO/Au device, with Au and W uniformly distributed in the top electrode. Scale bar: 10 nm. (d) Process flow of the ferroelectric capacitor fabrication. (e) EDS spectrum for analyzing the elemental ratio of alloy electrodes. Peaks for Cu stem from the copper grids. (f) EDS line scan result of the ferroelectric capacitor, once again validating the Au-W alloy/HZO/Au structure.

Table 1 Tuning the metal ratio and work function of alloy electrodes via adjusting the co-sputtering power

	Au	Au-W (1)	Au-W (2)	Au-W (3)	W
Co-sputtering power	–	Au: 150 W, W: 50 W	Au: 100 W, W: 100 W	Au: 75 W, W: 125 W	–
Atomic ratio of Au-W	1 : 0	0.787 : 0.213	0.482 : 0.518	0.198 : 0.802	0 : 1
Atomic percentage of W (%)	0	21.3	51.8	80.2	100
Work function (eV)	4.97	4.80	4.68	4.64	4.58

Figures 2(a) and (d).

The Au-W alloys were deposited by co-sputtering Au and W. The atomic ratio was adjusted by tuning the co-sputtering power (Table 1), which was measured by the energy-dispersive X-ray spectroscopy (EDS) shown in Figure 2(e). By gradually increasing the sputtering power of W and decreasing the sputtering power of Au, Au-W alloys with 21.3%, 51.8%, and 80.2% of W were realized. In this way, top electrodes with gradually increasing atomic percentage of W are achieved, as summarized in Table 1.

Due to the work function difference between Au and W, the Au-W alloy with different ratios may tune the work function simultaneously. Therefore, the Kelvin probe force microscopy (KPFM) was utilized to determine the work functions of electrode materials. A cleaved highly oriented pyrolytic graphite (HOPG) was used as a reference sample, whose work function is 4.60 eV [38]. The contact potential differences between the tip and electrode materials as well as HOPG were collected by KPFM. As a result, the work functions of five electrode materials were obtained and shown in Table 1, which monotonically decrease with the increase of W content. This result proves that the alloy-electrode method is able to tune the metal work function effectively.

The device structure is verified by the cross-sectional transmission electron microscopy (TEM) image shown in Figure 2(b), where the Au-W alloy/HZO/Au structure can be clearly observed. Lattice fringes in different directions can be observed in the HZO film, indicating polycrystalline HZO is obtained after annealing. The interface between the bottom Au electrode and HZO is relatively sharp, without significant interfacial layer formation. EDS mapping result presents that the Au and W elements are

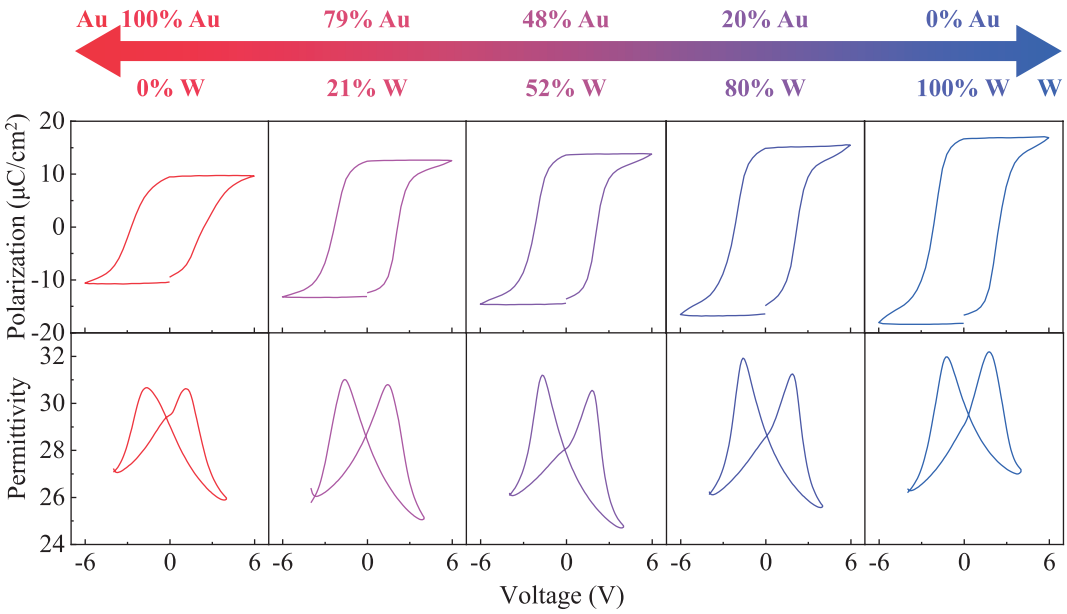

Figure 3 (Color online) With the alloy-electrode method, the ferroelectric polarization of the capacitors can be gradually tuned between the two baselines (100% Au and 100% W) as shown in the upper panel. The corresponding permittivity properties of different devices are shown in the lower panel, measured at 1 MHz with a small AC signal.

uniformly distributed in the top electrode, proving that Au-W alloy is successfully fabricated by co-sputtering (Figure 2(c)). Meanwhile, Hf, Zr, and O elements are also evenly distributed in the middle layer, showing a high-quality film grown by ALD (Figure 2(c)). The Au element is not observed in the middle layer, which ruled out the diffusion of Au during annealing. The three-layer structure is further verified by an EDS line scan in Figure 2(f), where clear boundaries between each layer can be observed.

Subsequently, the ferroelectric capacitors with varied top electrodes (varied α) were systematically measured using the positive-up-negative-down (PUND) method at the frequency of 1 kHz and amplitude of $+/-6$ V. The mechanical stress caused by the electrode has an important impact on the ferroelectric polarization of HZO, where the thermal expansion coefficient of electrode materials is crucial [31, 39]. As the α of electrode material decreases, the tensile stress of the HZO film increases, which results in a higher ratio of o-phase as well as stronger ferroelectric polarization in HZO [39]. Therefore, the capacitor with Au TE ($\alpha = 14.2 \times 10^{-6}$/K) presents the lowest $2P_{\rm r}$, while the capacitor with W TE ($\alpha = 4.5 \times 10^{-6}$/K) presents the highest $2P_{\rm r}$, as shown in the upper panel of Figure 3.

The thermal expansion coefficient of the alloy electrodes can be reasonably predicted by the rule of mixtures (ROM) model [40, 41]:

$$\alpha = \sum_{i=1}^{n} \alpha_i V_i, \tag{1}$$

where α is the thermal expansion coefficient of the alloy, α_i and V_i are the thermal expansion coefficient and volume fraction of each constituent. Eq. (1) indicates that electrode materials with different thermal expansion coefficients can be obtained by adjusting the ratio of alloy. In this example, via tuning the composition of Au-W alloy electrodes, the α can be gradually tuned from $\alpha_{\rm Au}$ to $\alpha_{\rm W}$ and therefore the ferroelectric polarization states between the two baselines can be obtained. Figure 4(a) exhibits the statistical results for TEs with increasing atomic percentage of W (0% to 100%), and as expected, the $2P_{\rm r}$ gradually increases from 20.7 to 31.8 μC/cm^2, which demonstrates the tuning ability of alloy electrodes. The permittivity properties of the ferroelectric capacitors were also measured and shown in the lower panel of Figure 3. The C-V characteristics of five capacitors all show typical butterfly curves and the dielectric constant slightly increases with higher W content in TE, corresponding to the P-V characteristics shown above.

It is worth mentioning that the alloy-electrode method is a general approach to tuning the ferroelectric polarization, where different metal combinations can be selected to fabricate alloy electrodes. For instance, the Cu-W alloy electrode is also realized in this work and demonstrated the ability to tune the ferroelectric polarization, as shown in Figure A1. The thermal expansion coefficients of Cu ($\alpha = 16 \times 10^{-6}$/K) and

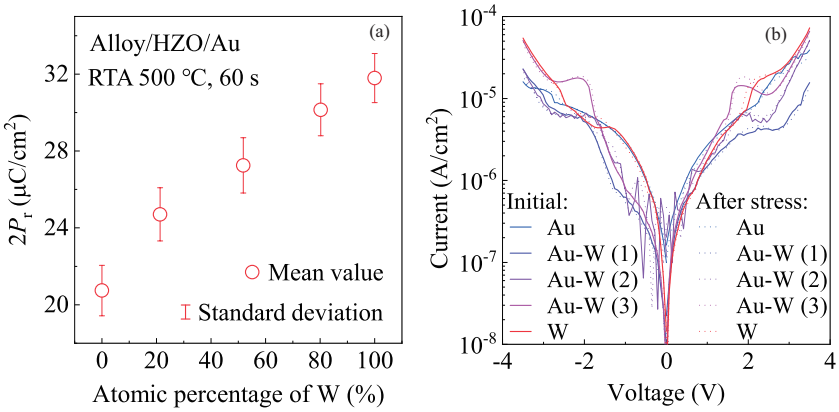

Figure 4 (Color online) (a) Remnant polarization of HZO improved with increasing atomic percentage of W in the alloy electrodes. Thirty devices were measured for each type of capacitor. (b) Leakage current for five types of capacitors before and after 10^5 cycling at 3.5 V.

W ($\alpha = 4.5 \times 10^{-6}$/K) are quite different, whereas their work functions are quite close. Therefore, the thermal expansion coefficient rather than the work function is adjusted in the Cu-W alloy, proving that the different thermal expansion coefficients are the main factor for tuning ferroelectric polarization in this example. Since the ferroelectricity of HZO can be effectively tuned by using materials with different thermal expansion coefficients in both top electrode and bottom electrode [39], the generality of the alloy-electrode method also lies in its applicability, which can be reasonably extended from top electrode to bottom electrode or both electrodes simultaneously. Moreover, the modulated characteristics are not limited to ferroelectric polarization, but can be extended to the leakage current, endurance, retention, and imprint of the device.

As discussed above, tuning the composition of alloy electrodes also results in the modulation of work function (Table 1), which will influence the leakage current of the capacitors. Figure 4(b) summarizes the leakage current of devices with different TEs before and after cycling. TEs with higher work functions help with the suppression of leakage current, such as Au, Au-W (1), and Au-W (2) electrodes. On the contrary, TEs with lower work functions show higher leakage currents, such as Au-W (3) and W electrodes. After 10^5 cycling, the leakage current for five types of capacitors was almost unchanged, showing stable defect density during 10^5 cycling.

The endurance characteristics of the fabricated capacitors were tested and the influences of electrode materials were evaluated. Ferroelectric capacitors were applied with 3.5 V voltage pulses at 100 kHz for 10^6 cycling, and the P-V loops were obtained by applying 5 V voltage sweeps at 10 kHz. Figure 5 exhibits the endurance characteristics of capacitors with different TEs, where the $2P_r$ gradually decreases with cycling and the wake-up effect is not observed for all devices. The capacitor with purely Au top electrode shows significant $2P_r$ drop for about 50% after 10^6 cycling (Figure 5(a)), which can be improved by adding W content into the Au electrode (Figures 5(b)–(e)). Since the leakage current does not increase obviously after 10^5 cycling (Figure 4(b)), which means the generation of oxygen vacancies is not significant, the observed fatigue effect should be attributed to the charge injection which results in the pinning of the domain wall and reduction of remnant polarization [42].

The different alloy-electrode compositions may have an influence on the retention characteristics of capacitors. Therefore, the retention tests for same-state (SS), new same-state (NSS), and opposite-state (OS) were carried out. For each type of device, four capacitors were used and different pulse sequences were applied [43]. The retention values up to 10^4 s were collected and calculated, as shown in Figures 6(a)–(e). All five types of devices show good retention characteristics, where the OS shows slightly a more obvious trend of degradation between 10^3 and 10^4 s. In comparison, the five types of capacitors do not show a clear trend of improvement, where the capacitor with W electrode exhibits the most stable retention characteristics. Since the capacitor with W electrode shows the strongest ferroelectric polarization and thus the highest o-phase fraction, the better retention may be due to the reduction of bulk depolarization field from the nonpolar phases [44].

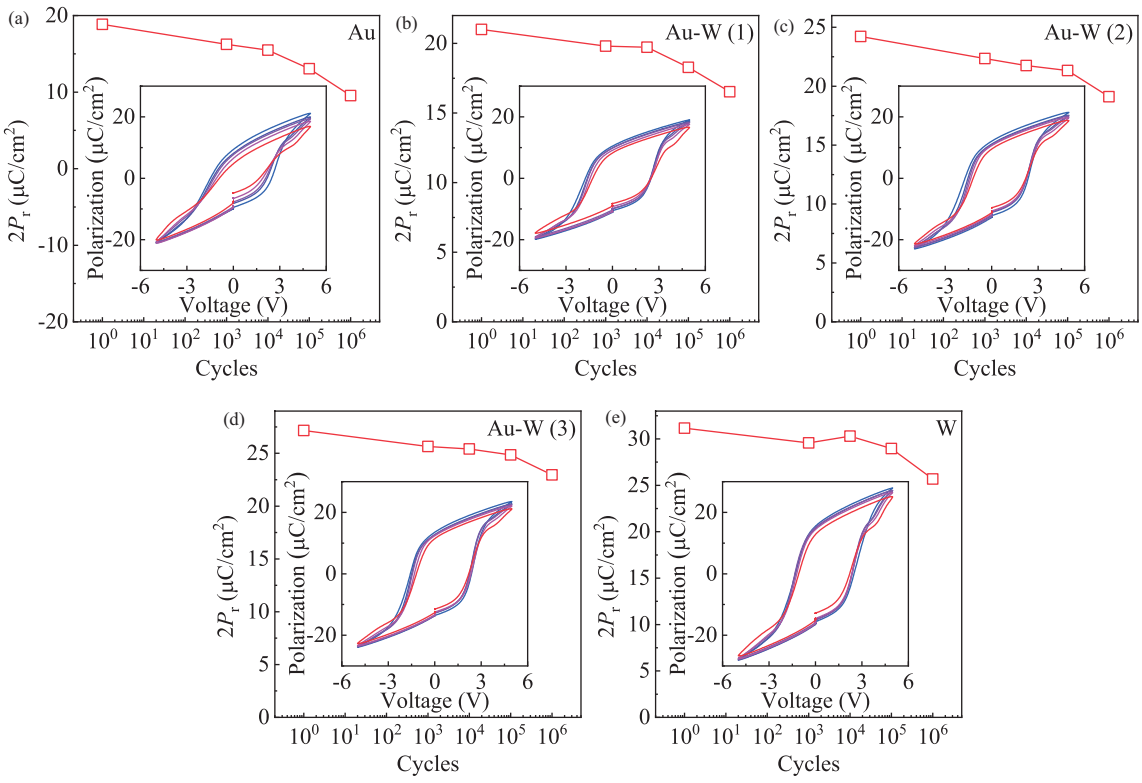

Figure 5 (Color online) Endurance and corresponding P-V characteristics of ferroelectric capacitors with (a) Au, (b) Au-W (21% W), (c) Au-W (52% W), (d) Au-W (80% W), and (e) W top electrodes.

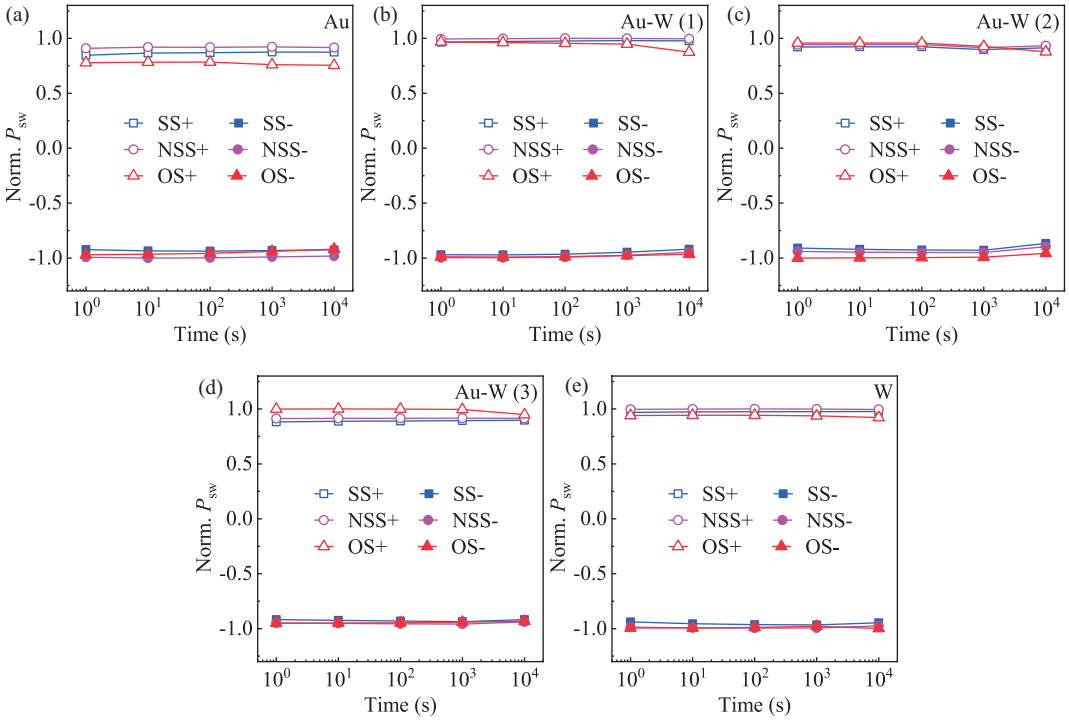

Figure 6 (Color online) Retention characteristics of ferroelectric capacitors with (a) Au, (b) Au-W (21% W), (c) Au-W (52% W), (d) Au-W (80% W), and (e) W top electrodes.

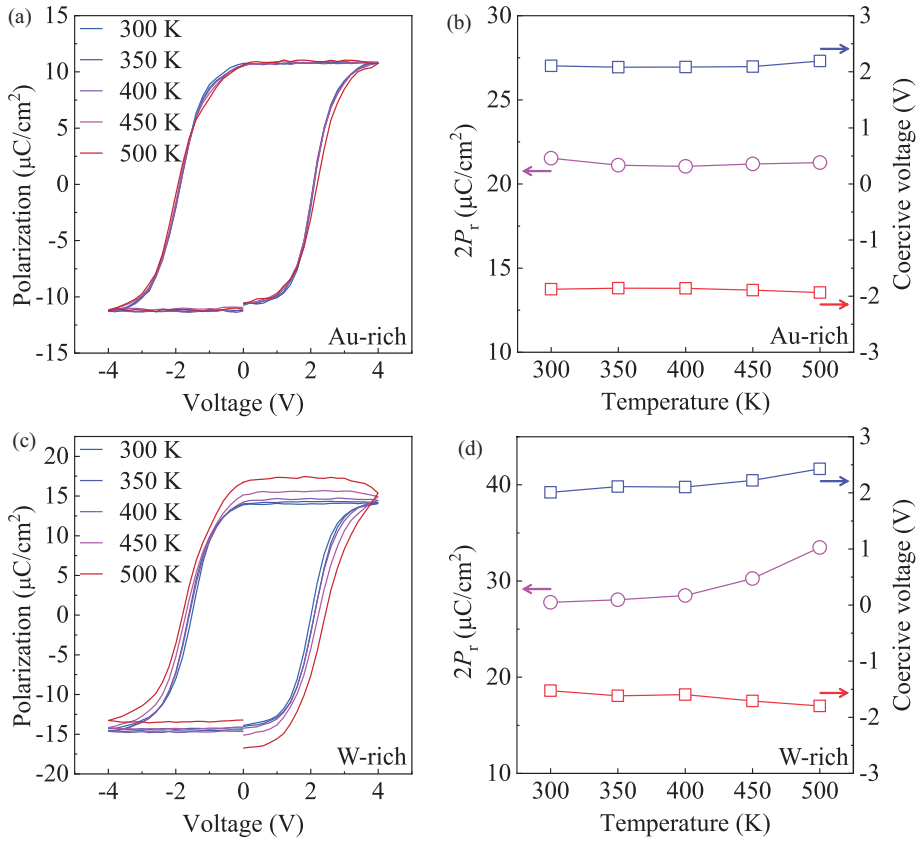

Figure 7 (Color online) *P-V* results of the Au-W alloy/HZO/Au capacitors with (a) Au-rich (79% Au) and (c) W-rich (80% W) top electrodes measured from 300 to 500 K. The extracted $2P_r$ and coercive voltages of Au-W alloy/HZO/Au capacitors with (b) Au-rich (79% Au) and (d) W-rich (80% W) top electrodes at different temperatures.

4 Temperature stability of ferroelectric capacitors

Temperature stability is of vital importance for HZO-based devices in real-world applications. When the temperature reaches the Curie temperature, HZO experiences a ferroelectric-paraelectric phase transition and $2P_r$ will decrease to zero. According to previous reports, Zr-doped HfO_2 exhibits a rather high Curie temperature (T_c = ~732 K, ~1203 K) [45,46].

To investigate whether HZO-based ferroelectric capacitors can work properly at high temperatures, the fabricated Au-W/HZO/Au capacitors with Au-rich (79% Au) and W-rich (80% W) TEs were chosen and measured with increasing temperatures. The PUND method was used and a voltage amplitude of $+/-4$ V was chosen to avoid capacitor breakdown at elevated temperatures. For capacitors with Au-rich top electrodes, the *P-V* loops exhibit typical ferroelectric hysteresis with very limited changes as the temperature varied from 300 to 500 K (Figure 7(a)), where the $2P_r$ and coercive voltages were extracted and shown in Figure 7(b). Since 500 K is sufficiently lower than the Curie temperature of HZO, $2P_r$ only slightly decreases as the temperature increases. On the other hand, the top (Au-rich) and bottom (Au) electrodes are relatively inert materials compared with TiN, with fewer oxygen vacancies at the electrode/HZO interface [47], resulting in a less significant shift of coercive voltages during high-temperature measurements (Figure 7(b)). Meanwhile, the *P-V* loops for the capacitors with W-rich top electrodes were also tested from 300 to 500 K. The capacitor can work stably below 450 K, but the hysteresis loops expand from 450 to 500 K, as shown in Figure 7(c). Since the $2P_r$ and coercive voltages are expected to decrease with increasing temperatures, the rising $2P_r$ and coercive voltages in Figure 7(d) are due to the increase of leakage current. The lower work function of the W-rich electrode as well as ion migration results in a more significant leakage current at elevated temperatures. The analysis above reveals that the fabricated HZO ferroelectric capacitors with W-rich and Au-rich top electrodes are able to work at temperatures up to 450 and 500 K, respectively, without significant change of $2P_r$ and shift of coercive voltages.

To further characterize the stability of fabricated HZO capacitors, the devices were baked at an elevated

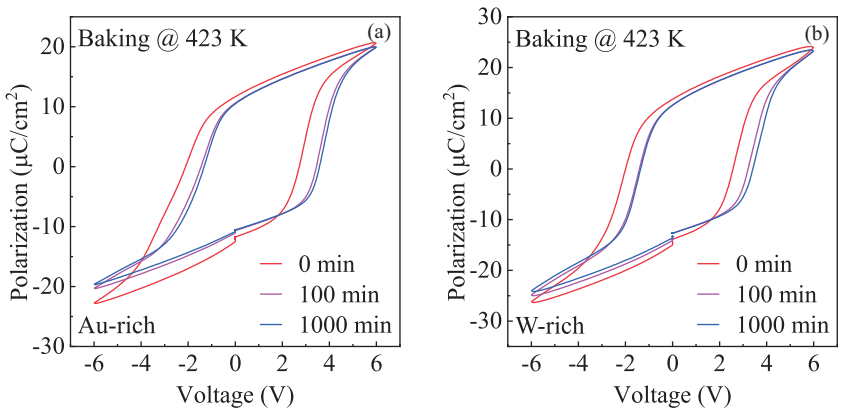

Figure 8 (Color online) Imprint tests for the Au-W alloy/HZO/Au capacitors with (a) Au-rich (79% Au) and (b) W-rich (80% W) top electrodes baked at 423 K for 0, 100, and 1000 min.

temperature for a long time to explore the imprint phenomenon which may severely affect the read-out reliability. The HZO capacitors with Au-rich and W-rich TEs were chosen and tested after baking at 423 K [47] for 0, 100, and 1000 min, as shown in Figures 8(a) and (b). Both types of capacitors reveal that the imprint phenomenon mainly happens within the first 100 min and gradually becomes stable from 100 to 1000 min. The Au-W alloy/HZO/Au capacitors have shown a positive shift of coercive field for ∼0.5 MV/cm, exhibiting a less significant imprint phenomenon compared with that of TiN/HZO/TiN capacitors (∼1 MV/cm) [47]. Owing to the less significant shift of the coercive field, the degradation of $P_{\rm r}$ is also limited. The imprint phenomenon originates from the electron de-trapping from oxygen vacancies at the TiN/HZO interface and the formation of a built-in electric field [47]. In this work, by replacing the TiN electrode with relatively electrochemically inert materials, the formation of TiO_xN_{1-x} interfacial layer is avoided, thereby alleviating the imprint phenomenon of HZO capacitors.

5 Conclusion

In this work, an alloy-electrode method is proposed and gradual tuning of ferroelectric polarization between two baselines is demonstrated, where the $2P_{\rm r}$ increases with increasing atomic percentage of W in the Au-W and Cu-W alloys. The ratio of the alloy electrodes also affects the leakage current, endurance, and retention of the devices. The HZO capacitors can sustain high temperatures up to 500 K with limited $2P_{\rm r}$ degradation and coercive voltage shift. A less significant imprint effect was observed thanks to the relatively inert electrodes. Such tunability and stability on ferroelectric polarization could facilitate the application of HZO in in-memory and neuromorphic computing.

Acknowledgements This work was supported by National Key R&D Program of China (Grant No. 2023YFB4502200), National Natural Science Foundation of China (Grant Nos. 61925401, 92064004, 61927901, 8206100486, 92164302), Beijing Natural Science Foundation (Grant No. L234026), and 111 Project (Grant No. B18001). Yuchao YANG acknowledges the support from the Fok Ying-Tong Education Foundation and the Tencent Foundation through the XPLORER PRIZE. Keqin LIU acknowledges the support from the China Postdoctoral Science Foundation (Grant Nos. 2023M740051, GZC20230046).

Supporting information Figure A1. The supporting information is available online at info.scichina.com and link.springer.com. The supporting materials are published as submitted, without typesetting or editing. The responsibility for scientific accuracy and content remains entirely with the authors.

References

1 Cheema S S, Kwon D, Shanker N, et al. Enhanced ferroelectricity in ultrathin films grown directly on silicon. Nature, 2020, 580: 478–482
2 Lee H J, Lee M, Lee K, et al. Scale-free ferroelectricity induced by flat phonon bands in HfO_2. Science, 2020, 369: 1343–1347
3 Bae H, Moon T, Nam S G, et al. Ferroelectric diodes with sub-ns and sub-fJ switching and its programmable network for logic-in-memory applications. In: Proceedings of IEEE Symposium on VLSI Technology (VLSI), 2021
4 Yuan R, Ma M Y, Xu L Y, et al. Efficient 16 Boolean logic and arithmetic based on bipolar oxide memristors. Sci China Inf Sci, 2020, 63: 202401
5 Kim M K, Lee J S. Ferroelectric analog synaptic transistors. Nano Lett, 2019, 19: 2044–2050
6 Jerry M, Pai-Yu C, Jianchi Z, et al. Ferroelectric FET analog synapse for acceleration of deep neural network training. In: Proceedings of IEEE International Electron Devices Meeting (IEDM), 2017

7 Liu K, Zhang T, Dang B, et al. An optoelectronic synapse based on α-In_2Se_3 with controllable temporal dynamics for multimode and multiscale reservoir computing. Nat Electron, 2022, 5: 761–773

8 Zhou H J, Li Y, Miao X S. Low-time-complexity document clustering using memristive dot product engine. Sci China Inf Sci, 2022, 65: 122410

9 Cheng C D, Tiw P J, Cai Y M, et al. In-memory computing with emerging nonvolatile memory devices. Sci China Inf Sci, 2021, 64: 221402

10 Zhu Y, He Y L, Chen C S, et al. IGZO-based neuromorphic transistors with temperature-dependent synaptic plasticity and spiking logics. Sci China Inf Sci, 2022, 65: 162401

11 Böscke T S, Müller J, Bräuhaus D, et al. Ferroelectricity in hafnium oxide thin films. Appl Phys Lett, 2011, 99: 102903

12 Böscke T S, Teichert S, Bräuhaus D, et al. Phase transitions in ferroelectric silicon doped hafnium oxide. Appl Phys Lett, 2011, 99: 112904

13 Mueller S, Mueller J, Singh A, et al. Incipient ferroelectricity in Al-doped HfO_2 thin films. Adv Funct Mater, 2012, 22: 2412–2417

14 Zhou J, Zhou Z, Jiao L, et al. Al-doped and deposition temperature-engineered HfO_2 near morphotropic phase boundary with record dielectric permittivity (∼68). In: Proceedings of IEEE International Electron Devices Meeting (IEDM), 2021

15 Olsen T, Schröder U, Müller S, et al. Co-sputtering yttrium into hafnium oxide thin films to produce ferroelectric properties. Appl Phys Lett, 2012, 101: 082905

16 Müller J, Schröder U, Böscke T S, et al. Ferroelectricity in yttrium-doped hafnium oxide. J Appl Phys, 2011, 110: 114113

17 Müller J, Böscke T S, Schröder U, et al. Ferroelectricity in simple binary ZrO_2 and HfO_2. Nano Lett, 2012, 12: 4318–4323

18 Müller J, Böscke T S, Bräuhaus D, et al. Ferroelectric $Zr_{0.5}Hf_{0.5}O_2$ thin films for nonvolatile memory applications. Appl Phys Lett, 2011, 99: 112901

19 Park M H, Kim H J, Kim Y J, et al. Evolution of phases and ferroelectric properties of thin $Hf_{0.5}Zr_{0.5}O_2$ films according to the thickness and annealing temperature. Appl Phys Lett, 2013, 102: 242905

20 Peng Y, Wang Z, Xiao W, et al. Effect of thickness scaling on the switching dynamics of ferroelectric HfO_2-ZrO_2 capacitors. Ceramics Int, 2022, 48: 28489–28495

21 Lin Y D, Lee H Y, Tang Y T, et al. 3D scalable, wake-up free, and highly reliable FRAM technology with stress-engineered $HfZrO_x$. In: Proceedings of IEEE International Electron Devices Meeting (IEDM), 2019

22 Peng Y, Xiao W, Liu Y, et al. HfO_2-ZrO_2 superlattice ferroelectric capacitor with improved endurance performance and higher fatigue recovery capability. IEEE Electron Device Lett, 2022, 43: 216–219

23 Gong Z, Chen J, Peng Y, et al. Physical origin of the endurance improvement for HfO_2-ZrO_2 superlattice ferroelectric film. Appl Phys Lett, 2022, 121: 242901

24 Liang Z, Tang K, Dong J, et al. A novel high-endurance FeFET memory device based on ZrO_2 anti-ferroelectric and IGZO channel. In: Proceedings of IEEE International Electron Devices Meeting (IEDM), 2021

25 Yoong H Y, Wu H, Zhao J, et al. Epitaxial ferroelectric $Hf_{0.5}Zr_{0.5}O_2$ thin films and their implementations in memristors for brain-inspired computing. Adv Funct Mater, 2018, 28: 1806037

26 Fujii S, Kamimuta Y, Ino T, et al. First demonstration and performance improvement of ferroelectric HfO_2-based resistive switch with low operation current and intrinsic diode property. In: Proceedings of IEEE Symposium on VLSI Technology (VLSI), 2016

27 Park M H, Lee Y H, Kim H J, et al. Ferroelectricity and antiferroelectricity of doped thin HfO_2-based films. Adv Mater, 2015, 27: 1811–1831

28 Luo Q, Cheng Y, Yang J, et al. A highly CMOS compatible hafnia-based ferroelectric diode. Nat Commun, 2020, 11: 1391

29 Karbasian G, dos Reis R, Yadav A K, et al. Stabilization of ferroelectric phase in tungsten capped $Hf_{0.8}Zr_{0.2}O_2$. Appl Phys Lett, 2017, 111: 022907

30 Zacharaki C, Tsipas P, Chaitoglou S, et al. Very large remanent polarization in ferroelectric $Hf_{1-x}Zr_xO_2$ grown on Ge substrates by plasma assisted atomic oxygen deposition. Appl Phys Lett, 2019, 114: 112901

31 Cao R R, Wang Y, Zhao S J, et al. Effects of capping electrode on ferroelectric properties of $Hf_{0.5}Zr_{0.5}O_2$ thin films. IEEE Electron Device Lett, 2018, 39: 1207–1210

32 Lin Y C, McGuire F, Franklin A D. Realizing ferroelectric $Hf_{0.5}Zr_{0.5}O_2$ with elemental capping layers. J Vacuum Sci Tech B, 2018, 36: 011204

33 Goh Y, Jeon S. The effect of the bottom electrode on ferroelectric tunnel junctions based on CMOS-compatible HfO_2. Nanotechnology, 2018, 29: 335201

34 Shiraishi T, Katayama K, Yokouchi T, et al. Impact of mechanical stress on ferroelectricity in $(Hf_{0.5}Zr_{0.5})O_2$ thin films. Appl Phys Lett, 2016, 108: 262904

35 Si M, Saha A K, Gao S, et al. A ferroelectric semiconductor field-effect transistor. Nat Electron, 2019, 2: 580–586

36 Zhou Y, Wu D, Zhu Y, et al. Out-of-plane piezoelectricity and ferroelectricity in layered α-In_2Se_3 nanoflakes. Nano Lett, 2017, 17: 5508–5513

37 Han W, Zheng X, Yang K, et al. Phase-controllable large-area two-dimensional In_2Se_3 and ferroelectric heterophase junction. Nat Nanotechnol, 2023, 18: 55–63

38 Melitz W, Shen J, Lee S, et al. Scanning tunneling spectroscopy and Kelvin probe force microscopy investigation of Fermi energy level pinning mechanism on InAs and InGaAs clean surfaces. J Appl Phys, 2010, 108: 023711

39 Lee Y, Goh Y, Hwang J, et al. The influence of top and bottom metal electrodes on ferroelectricity of hafnia. IEEE Trans Electron Devices, 2021, 68: 523–528

40 Dong N, Wang J, Ma H, et al. Effects of Nd content on thermal expansion behavior of Mg-Nd alloys. Mater Today Commun, 2021, 29: 102894

41 Bruck H A, Rabin B H. Evaluation of rule-of-mixtures predictions of thermal expansion in powder-processed Ni-Al_2O_3 composites. J Am Ceramic Soc, 1999, 82: 2927–2930

42 Chen L, Liang Z, Shao S, et al. First direct observation of the built-in electric field and oxygen vacancy migration in ferroelectric $Hf_{0.5}Zr_{0.5}O_2$ film during electrical cycling. Nanoscale, 2023, 15: 7014–7022

43 Mueller S, Muller J, Schroeder U, et al. Reliability characteristics of ferroelectric Si:HfO_2 thin films for memory applications. IEEE Trans Device Mater Relib, 2013, 13: 93–97

44 Mehmood F, Hoffmann M, Lomenzo P D, et al. Bulk depolarization fields as a major contributor to the ferroelectric reliability performance in lanthanum doped $Hf_{0.5}Zr_{0.5}O_2$ capacitors. Adv Mater Inter, 2019, 6: 1901180

45 Wang Y, Wang Q, Zhao J, et al. A robust high-performance electronic synapse based on epitaxial ferroelectric $Hf_{0.5}Zr_{0.5}O_2$ films with uniform polarization and high Curie temperature. Appl Mater Today, 2022, 29: 101587

46 Schroeder U, Mittmann T, Materano M, et al. Temperature-dependent phase transitions in $Hf_xZr_{1-x}O_2$ mixed oxides: indications of a proper ferroelectric material. Adv Elect Mater, 2022, 8: 2200265

47 Yuan P, Mao G Q, Cheng Y, et al. Microscopic mechanism of imprint in hafnium oxide-based ferroelectrics. Nano Res, 2022, 15: 3667–3674